Progress in Design and Fabrication of Resonator Quantum Well Infrared Photodetectors (R-QWIP)

Jason Sun, K. K. Choi, K. Olver and Rich Fu

Electro-Optics and Photonics Division

U.S. Army Research Laboratory

Adelphi, MD 20783, USA

E-mail: guifu.n.sun.civ@mail.mil; kwong.k.choi.civ@mail.mil; kimberley.a.olver.civ@mail.mil; richard.x.fu.civ@mail.mil

Abstract—**Resonator-Quantum Well Infrared Photo detectors (R-QWIPs) are the next generation of QWIP detectors that use resonances to increase the quantum efficiency (QE). Collaborating with L-3 Communications - Cincinnati Electronics, recently we explore R-QWIPs for long wavelength applications. By using our two optimized inductively coupled plasma (ICP) etching processes, two format (1Kx1K and 40x40) R-QWIP detectors were fabricated successfully. We achieved a quantum efficiency of 37% for 19 quantum wells and 35% for 8 quantum wells under a doping density of 0.5×10^{18} cm^{-3}. The cutoff wavelength and bandwidth of both detectors are 10.5 μm and 2 μm respectively. The thermal sensitivity of the large format FPA is 27.2 mK at half well-fill (Nw/2) of 8.85 M electrons and intergration time of 4.46 ms under F/2.5 optics.**

Keywords-QWIP; resonance; FPA; electromagnetic modeling; quantum efficiency; inductively coupled plasma (ICP) etching; GaAs substrate removal.

I. INTRODUCTION

We established a highly reliable electromagnetic (EM) model to calculate the quantum efficiency (QE) of an infrared detector [1]. We subsequently applied it to design a new detector structure, which is referred to as the resonator-QWIP (R-QWIP) [2]. An R-QWIP consists of an active quantum well (QW) layer, a GaAs bottom contact layer, and a top GaAs contact layer. On the top contact layer, there is an array of diffractive elements (DEs) that are covered with ohmic metal and gold layers. The ohmic metal consists of Pd/Ge/Au layers. The mesa is surrounded by a low index material, such as epoxy, and the substrate underneath the ground contact layer is completely removed.

When light is incident from the bottom side of the detector, it is scattered by the DEs back to the detector volume, and the subsequent angles of incidence are larger than the critical angles for total internal reflection at all detector boundaries. The light is therefore trapped inside the pixel. By designing a properly sized detector volume, the trapped light forms a constructive interference pattern, with which the internal optical intensity is greatly increased, thereby yielding a large QE. To achieve the expected performance, the height of the DE and the thickness of the active resonator must be uniformly and accurately realized to within 0.05 μm accuracy and the substrates of the detectors have to be removed totally to prevent the escape of unabsorbed light in the detectors. To achieve these specifications, an inductively coupled plasma (ICP) etching tool is used to fabricate a good number of test detectors and
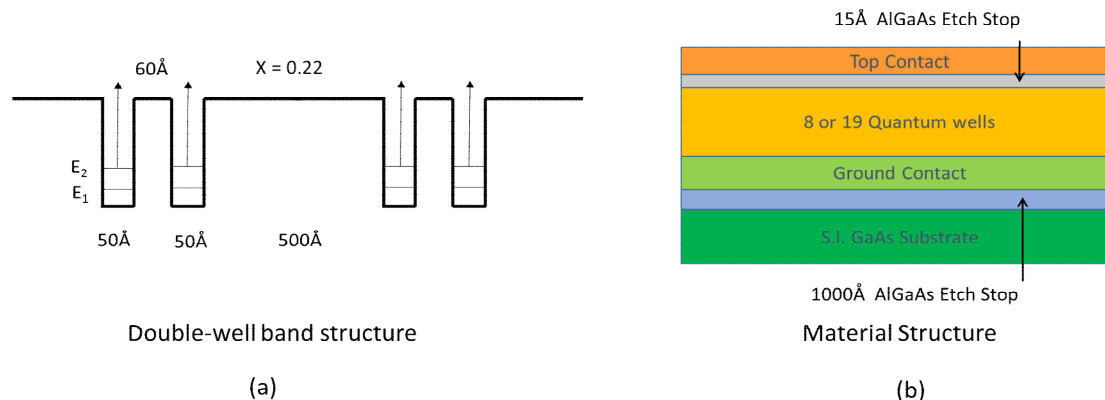

Figure 1. (a) The band structure of double-well QWIP material design. (b) The material layer structure.

FPAs. In an inductively coupled plasma (ICP) system, ion density is controlled by ICP source power alone. Increasing ICP source power increases ion density. Meanwhile, ion energy is affected by both ICP source power and RF chuck power. Increasing ICP power decreases induced dc bias. On the contrary, increasing RF chuck power raises dc bias on the chuck. Since an ICP system provides one more process parameter than a reactive ion etching (RIE) system for plasma control, it is more flexible to use ICP to optimize different etching processes, such as selective (etching GaAs over AlxGa1-xAs stop etching layer) versus non-selective etching, or isotropic versus vertical etching [3-7]. We thus

adopted ICP etching (selective and non-selective) over reactive ion etching (RIE) for the fabrication of test detectors and FPAs. Our selective ICP etching process can yield a very high selectivity (>5000:1) and a fast GaAs etching rate (2700Å/min). The etching surface was perfectly smooth and mirror-like after processing. In addition to high selectivity and smooth etching surface, the process is also highly reproducible and shows no damage to the detector material [8-11].

In this work, we designed an R-QWIP with a broad resonance. When it couples to a broadband material, which has a cutoff wavelength at 10.5 µm, infrared radiation between 7.5 – 10.5 µm within the long wavelength infrared (LWIR) window can be efficiently detected. Two format R-QWIP detectors were fabricated (1K x 1K and 40 x 40). The pixel pitch size are 20 µm and 25 µm respectively. In this article, we will describe the material and geometry design, fabrication and test results.

II. 10.5 µM CUTOFF R-QWIP DESIGN

To design a broadband R-QWIP with 10.5 µm cutoff, we use a double-well structure to broaden the spectral bandwidth of the QWIP material. In the design, each quantum well (QW) period contains a 50-Å GaAs QW, a thin 60-Å $Al_{0.22}Ga_{0.78}As$ barrier, another 50-Å GaAs QW, followed by a thick 500-Å $Al_{0.22}Ga_{0.78}As$ barrier. To reduce the dark current level in this long wavelength detector, a moderate doping density N_D of 0.5×10^{18} cm^{-3} is adopted for each QW. If the two GaAs QWs are coupled through the thin barrier, its bandwidth is broadened from ~1 µm to ~3 µm. Figure 1 (a) shows the band structures of the design. Figure 1 (b) shows the material layer structure. Two types of wafer materials are subsequently grown, 19 QW periods and 8 QW periods. They are labeled as DX1 and DX2. The active layer thickness of DX1 and DX2 are 1.3 µm, and 0.6 µm respectively.

Figure 2(a) shows the R-QWIP geometry design. Each pixel consists of 9 GaAs rings as diffractive elements (DEs) that covered with ohmic metal and gold. The pixel size is 20 × 20 µm^2 with a 25-µm pixel pitch. In this structure, the incident light is diffracted by the DEs and reflected back to the active layer as shown in Figure 2(b) where it is trapped and circulated inside the pixel until it is absorbed eventually.

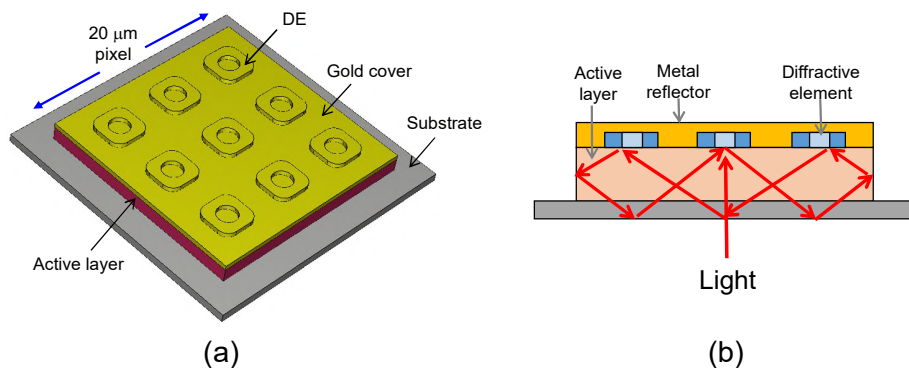(a)   (b)

Figure 2. (a) The optimized R-QWIP geometry for the 7.7 – 10.5 µm band. (b) The schematic light path inside the detector.

III. R-QWIP FABRICATION

R-QWIP focal plane array (FPA) and test detector fabrication process involves five masks. We use the first mask to create an array of rings as DEs. By using an EVG 120 Resist Processing Cluster, 1.8µm thick AZ5214 photoresist was coated on the wafers. The resist was baked at 110C° for one minute in the system. Karl Suss MA/BA6 Contact Aligner was used to expose photoresist and align patterns over layers. The DEs were formed by using our optimized selective ICP etching process to etch down to the 15 Å etch-stop layer, which is shown in picture 1(b). The optimized etching parameters were: BCl3 = 20 sccm, SF6 = 10 sccm, Ar = 10 sccm; pressure = 0.5 mTorr; RF Power = 0 W; ICP Power = 200W; and substrate temperature = 25˚C. Before the ICP etching, one minute oxygen plasma was used to clean the etching surface. The etching process was conducted in a Unaxis VLR 700 Etch System. Since the selective etching process has a very high selectivity (greater than 5000:1 for $Al_{0.4}Ga_{0.6}As$), 15-Å thick stop etching layer is sufficient to define the DE height. The etch-stop layer is also important to maintain a uniform height across the wafer as the etching rate is higher near the wafer edge. Figure 3 shows a microscope pictures that was taken after DE etching.
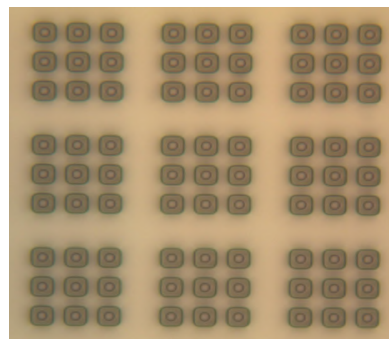

Figure 3. A microscope picture taken after DE etching.

We use second mask to delineate the ground contact area located outside the detector area. Optimized non-selective ICP etching recipe was used to touch the ground contact layer. The etching parameters were: BCl3 = 50 sccm, Ar = 10 sccm; pressure = 5 mTorr; RF Power = 80 W; ICP Power = 800W; and substrate temperature = 25˚C. In this etching, we apply a finite RF power to form a vertical sidewall. Since The RF power also induces a DC voltage on the chuck, which accelerates the ions toward the etching material, we minimized the RF power to avoid the possible plasma damage.

In metallization step, instead of negative photoresist, we use positive photoresist to create a favorable undercut for metal lift-off. In our case, the DE elements scatter UV light during exposure, which results in the undercut. The metal layer consists of five layers of materials, and they are: Pd(50Å)/ Ge(200Å)/ Au(300Å)/ Pd(50Å)/ Au(5000Å). After lift-off, the wafer was annealed in a tube furnace at 350C for 25 minutes.

The fourth mask was used to define the pixels. We opened the pixel areas while other areas were covered with photoresist. In the pixel areas, the metal pads were used as etching masks, and non-selective ICP etching was utilized to create individual pixels. The fifth mask is indium bump mask. We coated 9 μm-thick positive photoresist (AZ9245) and deposited 5 μm-tall indium bumps on the wafer using a thermal evaporator. Figure 4. Shows a microscope picture taken after indium bump deposition. The wafer was then diced into FPAs and test detectors and candidates were bump bonded to readout and fanout circuits. The backsides of the detectors were then filled with low viscosity epoxy.
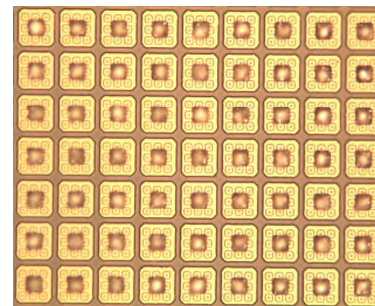

Figure 4. A microscope picture taken after indium bump deposition (1K x 1K format and 25 μm pixel pitch size).

One of the most important process step is substrate removal. Thinned QWIP FPAs offers several advantages over un-thinned detector FPAs. Besides other general benefits, substrate removal is specifically important for R-QWIP. The thinned R-QWIP FPAs and test detectors enhance the resonant effects, and the QE can rise by a factor of 3 - 5 according to EM modeling. To remove the substrate of FPAs and test devices, we need to mechanically lap the substrates to within 50 μm. Our optimized selective etching process was then use to totally remove the substrates. The surface of the dies is uniform, smooth and mirror-like after etching.[8]

IV. DX1 (19 QWs) R-QWIP CHARACTERISTICS

The test detector of DX1 R-QWIPs are fabricated into groups of 40 × 40 pixel elements and they are hybridized to
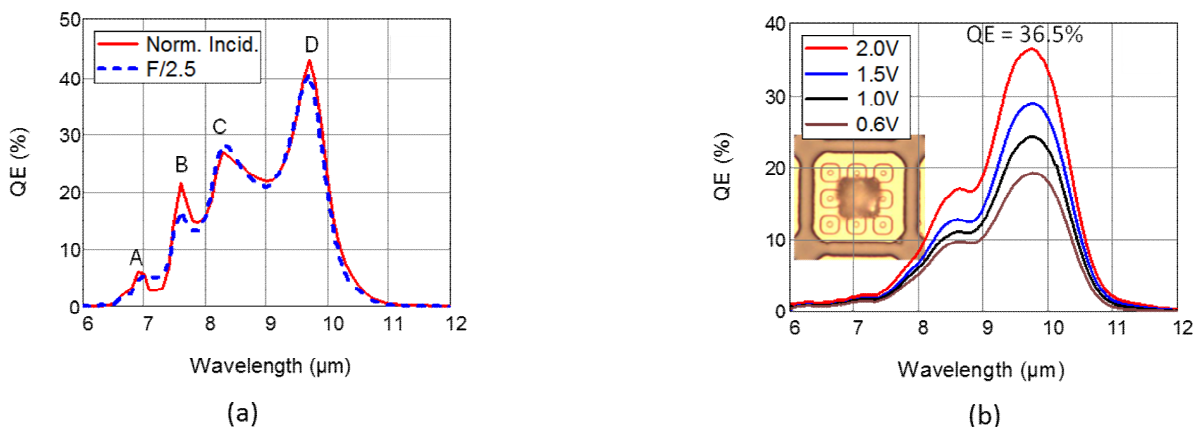

(a)

(b)

Figure 5. The calculated (a) and observed (b) QE of DX1 R-QWIP under positive substrate bias at T = 10 K. The insert shows the realized geometry, which is partly masked by an indium bump contact at the center.

fanout circuits. The fabricated pixel is shown in the insert of figure 5(b). After backfilling with epoxy, the substrate was removed completely. The conversion efficiency (CE) is measured at different substrate bias v at the operating temperature t = 10 K. The light source is a globar monochromator. Next, the gain of the detector is deduced from the noise measurements. From the values of CE and g,

the QE spectrum can be obtained and it is shown in figure 5(b). The maximum QE at 2 v is 36.5%. Figure 5(a) shows the expected QE spectrum for the present detector material and structural designs. If we assume a planar wave front as in normal incidence, the peak at 9.7 μm will have a QE of 43%. On the other hand, if we assume a spherical wave front as in f/2.5 optics, the main peak will be slightly

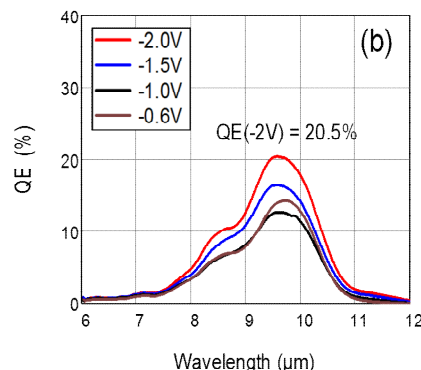reduced to 38%. The overall detection lineshape however   remains almost the same. Comparing the calculated and

Figure 6(a) The IR image taken by the DX1 FPA. (b) The deduced QE of DX1 under negative substrate bias at T = 10 K.

observed QE spectrum in Figure 5(a) and (b), the observed peaks are broader. These broader peaks may help to explain the slightly lower averaged peak value from the theoretical expectations. Even with the broadened peaks, the individual peaks from A to D are still visible at the calculated wavelengths, although the magnitudes of A and B peaks are smaller than predicted. We attribute this peak suppression to the processing imperfections and nonuniformity. Since A and B are higher order resonances in the shorter wavelengths, their vertical electric polarization distributions have higher spatial frequencies and thus will be more sensitive to the fidelity of the global detector geometry. As seen in figure 4 and in the insert of figure 5(b), the fabricated pixel has rounded corners and the rings are slightly displaced from the pixel center, both are deviated from the EM model. These imperfections may be the causes for the lower peaks.

Although QE under positive substrate bias is consistent with EM modeling, QE under negative bias is substantially smaller, and it is shown in Figure 6(b). Under negative bias, QE at -2 V are 20.5%. It is nearly a factor of 2 less than that under positive bias. The same situation was also observed in three separate wafer materials in earlier studies. We attribute this polarity asymmetry to the fact that the resonant optical intensity is highly localized along the z axis. The value of vertical optical intensity decreases exponentially from the maximum at the top of the active layer to zero at the bottom of the ground contact layer. This highly localized intensity makes the creation of photocurrent sensitive to the internal potential drop across the QWs. It is known that the potential drop inside a QWIP is not linear but larger at the cathode than at the anode. The photoelectrons generated at the cathode are then more likely to drift out of the well and contribute to the photocurrent. The photoelectrons at the anode, on the other hand, are prone to recombine in the same well and do not create a photocurrent. Therefore, when the cathode is at the top of the QW layer under positive substrate bias, almost all optical absorptions generate photocurrent and thus the detection QE is closer to the absorption QE. Conversely, under negative substrate bias,

the anode situates in the high intensity region where the QWs are less active. The detection QE is thus reduced.

In addition to the fanout circuits, we also produced a DX1 focal plane array with the same pixel size and pitch in a 1-megapixel format. The FPA was first characterized in an experimental dewar using a globar monochormator. Figure 6(a) shows an infrared image taken in this experimental dewar. The FPA operating condition is: T = 61 K, V ~ -1.1 V, F/# = 2.5, integration time τ_{int} = 3.06 ms, and signal processing = 1-point background subtraction. Under this operating condition, the pixel operability is 99.5% and thermal sensitivity (NEΔT) is 45 mK. After this measurement, the FPA was integrated into a camera that can operate at a lower T. With a F/2.5 lens, 300 K background, 55 K cold stage T, and a lower bias of ~ -0.5 V, the measured NEΔT is 27.2 mK at half well-fill ($N_{w/2}$) of 8.85 Me$^-$ and integration time (τ_{int}) of 4.46 ms.

V. DX2 (8 QWs) R-QWIP CHARACTERISTICS

To confirm the explanation of the polarity asymmetry, we adopted the DX2 material structure, which has fewer QWs (8 QWs instead of 19 QWs) but has the same total thickness as DX1 so that they have the same resonant structure. In DX2, the original 1.3-μm thick active layer is divided into two material layers: a 0.6-μm thick active layer at the top and a 0.7-μm contact layer at the bottom.

Figure 7(a) shows QE of DX2 R-QWIP under positive bias. At 0.8 V, QE are 34.7%, which is only slightly less than the 36.5% for DX1. The similar QEs thus confirm that the vast majority of IR absorption indeed occurs within a very thin layer (< 0.6 μm) next to the diffractive elements. The nearly equal QE for different active thicknesses was predicted in a previous study[12] and is confirmed in this experiment. The photons cycle more times in less absorbing layers, thus yielding similar QE. Furthermore, the DX2 QE at negative bias of -0.8 V, shown in Fig. 7(b), is 33.8%, respectively. They are almost the same as that under positive bias, which again confirms that all DX2 QWs are in the high intensity region.
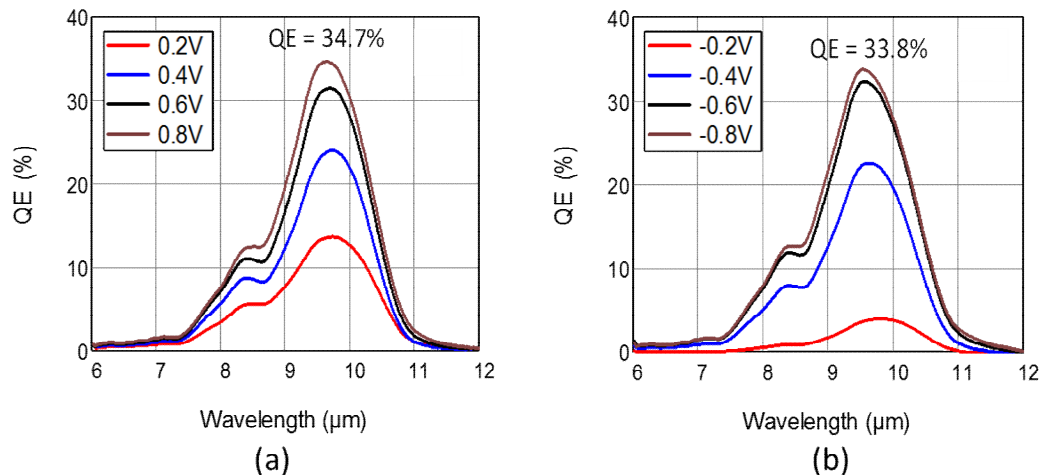

Figure 7 The QE spectra of the DX2 R-QWIP under positive substrate bias (a) and under negative substrate bias (b).

VI. CONCLUSION

We designed a broadband long wavelength R-QWIP detector. With the help of our two optimized ICP etching processes, we fabricated a good number of FPAs and test detectors. Using a moderate 0.5×10^{18} cm^{-3} doping, we achieved 37% QE in a 19-QW detector and 35% in an 8-QW detector at a large positive substrate bias. Similar QE can also be obtained under negative bias in the 8-QW detector. Despite the fact that the present readout circuit operates on negative bias, the DX1 FPA shows a thermal sensitivity of 27.2mK with 99.5% operability at 55 K under F/2.5 optics and 4.46 ms integration time. Higher sensitivity, shorter integration time, and higher operating temperature are expected at positive bias. With nearly double QE of DX2 relative to DX1 at negative bias, higher performance will also be expected from the DX2 FPA. To yield better R-QWIP performance under various operating conditions, we are studying single-well designs with different doping densities. Since contact mask allgner creates some pattern defects and non-uniformity, we are using a Step and Repeat (Stepper) Projection System to expose and align wafers, which will yield better resolution and more accurate alignment. The result will be reported elsewhere.

ACKNOWLEDGMENT

REFERENCES

[1] K. K. Choi et al., "Electromagnetic modeling and design of quantum well infrared photodetectors," IEEE J. Sel. Top. Quantum. Electron., vol. 19, pp.3800310(1)–3800310(10), 2013.

[2] K. K. Choi et al., "Resonator-quantum well infrared photodetectors," Appl. Phys. Lett., vol. 103, 201113(1)–201113(4), 2013.

[3] A. Mitchell, R. A. Gottscho, S. J. Pearton, and G. R. Schetler, "Real-time, in situ monitoring of GaAs and AlGaAs photoluminescence during plasma processing", Appl. Phys. Lett., vol. 56 (9), pp.821–823, 1990.

[4] C. M. Knoedler, L. Osterling, and H. Shtikman, "Reactive ion etching damage to GaAs Layers with etch stops," J. Vac. Sci. Technol., vol. B6, pp.1573-1576, 1988.

[5] S. J. Pearton et al., "Reactive ion etching of GaAs with CCl2F2:O2: Etch rates, surface chemistry, and residual damage," J. Appl. Phys., vol. 65, pp.1281-1292, 1989.

[6] T. R. Hayes, U. K. Chakrabarti, F. A. Baiocchi, and A. B. Emerson, "Damage to InP and InGaAsP surfaces resulting from CH4/H2 reactive ion etching", J. Appl. Phys., vol. 68, pp.785-792, 1990.

[7] J. W. Lee, M. W. Devre, B. H. Reelfs, D. Johnson, and J. N. Sasserath, "Advanced selective dry etching of GaAs /AlGaAs in high density inductively coupled plasmas", J. Vac. Sci. Technol., vol. A18, pp.1220-1224, 2000.

[8] J. Sun and K. K. Choi, M. D. Jhabvala, and C. Jhabvala, "Advanced Substrate Thinning Process for GaAs-Based Devices", J. Micro/Nanolith. MEMS MOEMS, vol.10(2), pp.023004(1)-023004(4), Apr–Jun 2011.

[9] Jason Sun, K. K. Choi, and Unchul Lee, "Fabrication of Pyramidal corrugated quantum well infrared photodetector focal plane arrays by inductively coupled plasma etching with BCl3/Ar", Journal of Micro/Nanolithography, MEMS, and MOEMS, vol.11(4), pp.043003(1)–044003(4), Oct–Dec 2012.

[10] Jason Sun, K. K. Choi, and K. Olver, "Fabrication of Resonator-quantum well infrared photodetector test devices", SPIE Journal of Micro/Nanolithography, MEMS, and MOEMS, Vol. 11(1), pp.013004(1)-013004(4), January 2014.

[11] Jason Sun, K. K. Choi, M. D. Jhabvala, C. A. Jhabvala, A. Waczynski and K. Olver, "Advanced Inductively Coupled Plasma Etching Processes for Fabrication of Resonator-Quantum Well Infrared Photodetector", Infrared Phys. Technol., Vol. 70, pp. 25–29, May 2015